NRIAG JOURNAL OF ASTRONOMY AND GEOPHYSICS
2019, VOL. 8, NO. 1, 55–72
https://doi.org/10.1080/20909977.2019.1615799

Thermal maturation assessment of multiple organic-rich intervals in the Khatatba Formation and its influences on hydrocarbon potentiality, North East Abu Gharadig Concession, elucidated by 1D basin modeling approach

Mohammed A. Ahmed [a] and Mostafa M. A. Hassan [b]

[a]Geology Department, Mansoura University, Mansoura City, Egypt; [b]Egyptian General Petroleum Corporation, New Maadi, Cairo, Egypt

ABSTRACT

Hydrocarbon generation and expulsion simulations of multiple organic-rich intervals with diverse kerogen types in the Khatatba Formation were performed. Generally, the organofacies exhibit an excellent generation potential for liquid hydrocarbons, gas plus oil and/or gas. The 1D forward approaches have been executed for the complex tectonic and basin-fill history. The spatial distribution of the Khatatba organofacies and allocation of significant discoveries from the Khatatba Formation are aligned perpendicular to the NE-SW Jurassic Fault System. The organic-rich intervals underwent several heating episodes throughout its burial history predominantly during the Cretaceous Rifting phase. Likewise, the organofacies underwent episodic expulsion of gas derived from either primary cracking (kerogen type III) or secondary cracking of oil (kerogen type II). The oil prone type II kerogen entered the oil window at JD-4 well close to the Albian whilst the wet-gas window since late Albian. Conversely, gas prone type III kerogen attained the dry-gas window from the time of early Oligocene at the JD-4 well prior to the wet-gas window of the JG-2 well (late Oligocene). Nevertheless, gas prone type III kerogen never reached the dry gas window at JG-2 well due to its low thermal maturation level. The burial effect, attributable to the thick basin-fill sediments (Masajid, Alam El Bueib, Abu Roash and Khoman formations), accelerated the thermal maturation at the JD-4 well. However, the organofacies revealed neither thermogenic gas generation nor gas secondary cracking at the JG-2 well and nix expulsion. The expelled hydrocarbon assumed to migrate laterally and near vertically from the southeastern part towards the north western part.

KEYWORDS

Basin Modelling; multiple organic; rich intervals; hydrocarbon-generation potential; thermal maturation assessment-Khatatba Formation; NEAG Concession

1. Introduction

The Western Desert has excellent hydrocarbon potentiality and well thought-out as a significant oil province in Egypt. The North East Abu Gharadig (NEAG) concession is located on the northeastern side of the Abu Gharadig basin (Figure 1). Tectonically, the north Western Desert lies in the unstable shelf, comprises 10 main basins, eight of which are Mesozoic, a Paleozoic (Faghur-Siwa) Basin and a Tertiary basin (Gindi Basin). Those Mesozoic basins are Shushan, Matruh, Kattaniya, Qattara, Dahab-Mireir, Natrun, Alamein and Abu Gharadig basins.

A complete well log interpretation plus geochemical evaluation of the multiple organic-rich intervals in the Khatatba Formation as well as hydrocarbon-bearing zones are implemented into a conceptual model to obtain in depth well-calibrated burial and thermal histories. The chief purpose is to simulate geological situations and assign the thermal maturation of the multiple organic–rich intervals of the Khatatba-Khatatba (known) petroleum system. A petroleum system includes an area of all known accumulations related to a specific pod of mature source rock (Magoon and Dow 1994). The core objectives going to: (1) simulate thermogenic hydrocarbon generation and expulsion of the organofacies; (2) identify the influences of each one on the others; and (3) recognise zones of liquid hydrocarbon along with gas generation windows. The construction and evaluation of the 1D approach were performed by means of PetroMod software®.

2. Geologic framework

The Abu Gharadig basin is the major basin in the north Western Desert. The basin is an asymmetrical intra-cratonic basin trending east-west (EGPC 1992) that may have initiated as pull-a-part basin flanked by two right lateral wrench faults (Meshref 1990). The Abu Gharadig basin was created in the Albian and attained its maximum subsidence during the Maastrichtian and subsequently inverted through Paleocene-Eocene (Lüning et al. 2004).

A major phase of folding affected the basin in Santonian time (RRI 1982) leading to the development of numerous northeast-southwest anticlines (Kostandi 1963). The (NEAG) concession is a complex faulted anticline bounded to the west and east by reverse faults (EGPC 1992). Northwards, it is bordered by faults downthrown that separate the

CONTACT Mohammed A. Ahmed ahmed5@mans.edu.eg Geology Department, Mansoura University, Mansoura City, Egypt

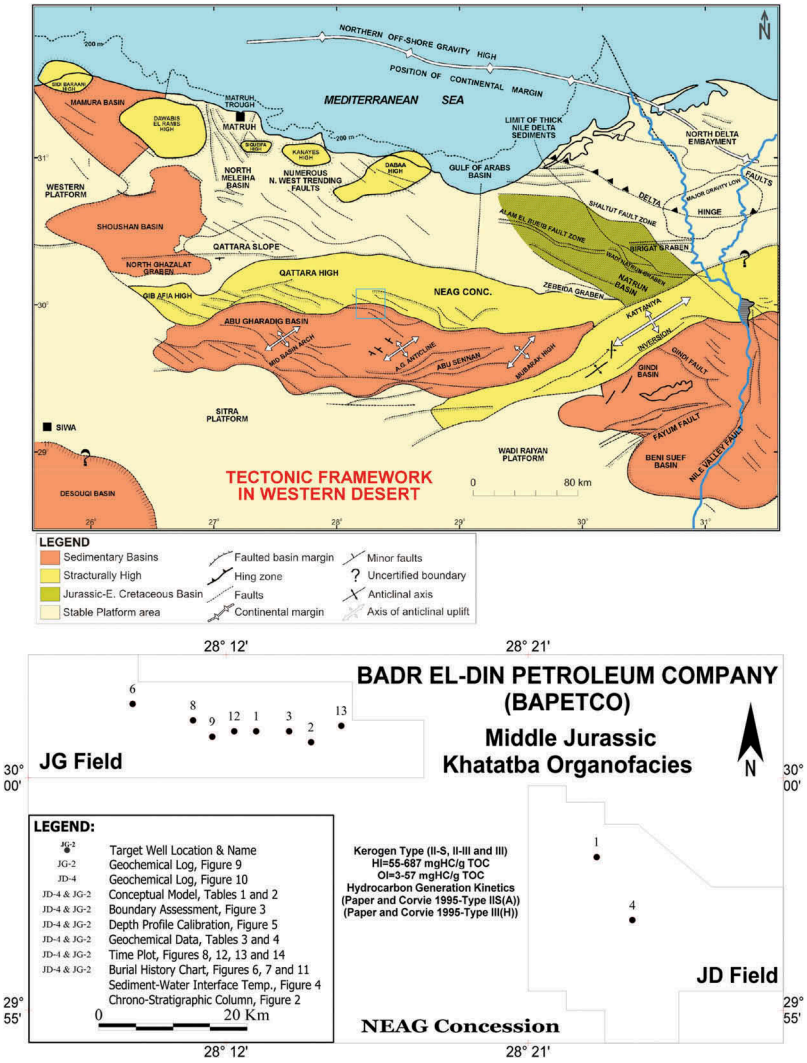

Figure 1. (A) 2-Dimensional index map showing the main east-west sedimentary basin and major tectonics in the north Western Desert, Egypt, modified after (Ahmed, 2008; Bayoumi 1996). (B) An enlarged location map of the study area (NEAG concession) illustrating the spatial distribution of the available 11 wells that belong to Badr El-Din Petroleum Company (**Bapetco**); nine wells drilled in the JG and two in the area of JD. The study area is located between longitudes 28° 27′ and 28° 6′E and latitudes 30° 04′ and 29°754′N. A total count of 11 wells; nine drilled in JG (JG-6, 8, 9, 12, 12 ST, 1 ST, 3, 2 ST and 13) and two in the area of JD (JD-1 ST and JD-4).

NEAG area from the Rabat structural high fault blocks. Structurally, the basin was affected by extensional deformation, throughout Jurassic and Cretaceous, and acquired half-graben geometry with northward tilting (Moustafa et al. 1998). Three normal fault trends: WNW-ESE, NE-SW and E-W are dominant (Moustafa 2008). While, reverse faults with ENE as well as E-W trends are relatively less abundant (Abd El Aal 1988). The E-W trend is suggested to be Jurassic-Early Cretaceous whilst the ENE is Jurassic (Meshref 1996). The anticlines along with the tilted fault blocks are bounded by early rift WNW-ESE and E-W faults that form the major hydrocarbon traps (Moustafa 2008) in several fields such as: BED, Sitra, north and northeast Abu Gharadig, El Faras, El Mohr, Raml, JG, JD and Raml.

The Middle Jurassic Khatatba Formation is overlain by the Late Jurassic Masajid Formation (Zobaa et al. 2013), as shown in Figure 2, and differentiated into six members from the top to the base as follows: Upper Safa A; Upper Safa B; Kabrit; Lower Safa A; Lower Safa B and Lower Safa C. The Khatatba Formation is one of the most prolific source rocks (oil, gas and mixed oil and gas prone) in the north Western Desert (Ahmed, 2008; EGPC 1992; Schlumberger 1995; Maky and Ramadan 2008; Shalaby et al. 2011; El Diasty 2015). The Khatatba organic-rich intervals proved to be effective source rocks (Maky and Ramadan 2008; Shalaby et al. 2011; El Diasty 2015). Furthermore, it exhibits excellent reservoir characterisation in the NEAG concession (Hassan et al. 2016).

3. Basin modelling procedure

The conceptual model, (Tables 1 and 2), represents a time-span numerical restoration of the (NEAG) concession through which one of three basic geologic processes dominated, that is accumulation of a layer

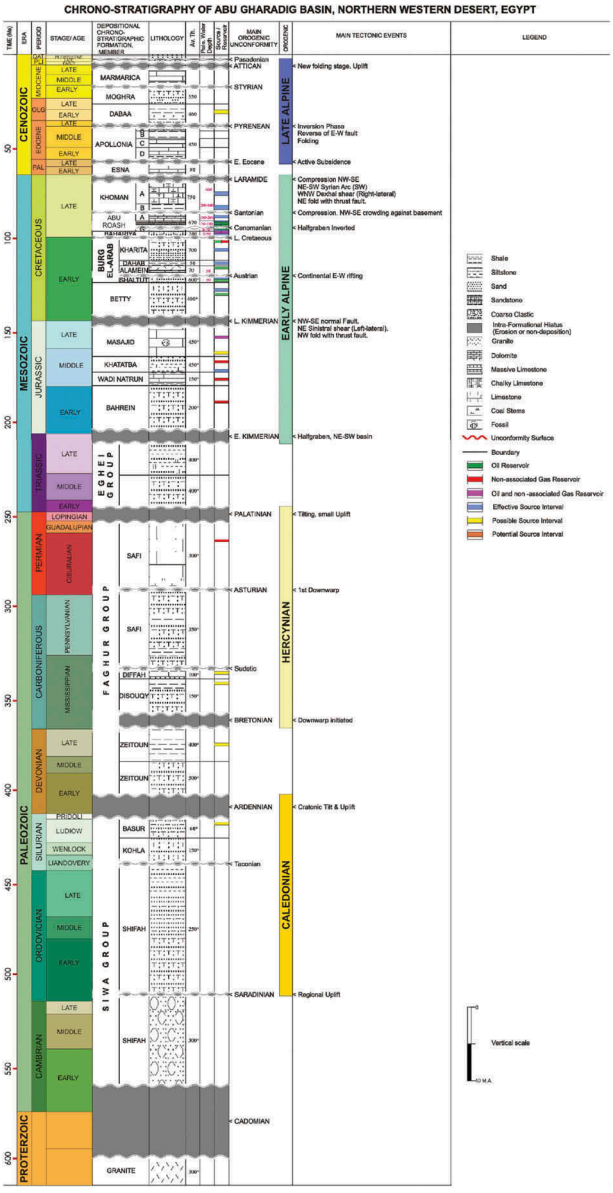

Figure 2. A generalized chrono-stratigraphic column and tectonic correlation chart of Abu Gharadig Basin, north Western Desert, Egypt (Ahmed, 2008). The facies succession, ages, distribution of potential source and reservoirs rocks are also represented, modified after (Schlumberger 1984, 1995; Guiraud and Bosworth 1999; Guiraud et al. 1999). The tentative paleowater depth is based on palynological and foraminiferal analysis of ditch samples for the Cretaceous age (Abd El Kireem et al. 1996). The average recorded thickness values are inferred from literature. The Geologic age scale is according to (Harland et al. 1990). The colour code is selected according to the United States Geological Survey (USGS).

(deposition), non-deposition (hiatus), or uplift and subsequent erosion (unconformity). The numerical simulation of the conceptual model throughout geologic time, based on physical and chemical reactions, is performed (Welte and Yükler 1981; Ungerer et al. 1990; Burrus et al. 1996). The foremost objective is to simulate the burial and thermal histories of the NEAG concession that influence thermal maturation, hydrocarbon generation, migration and accumulation. The thermal history depends on boundary conditions (Figure 3) that include the sediment-water interface temperature (SWIT, values in °C) and the paleo-heat flow (HF, values in mW/m^2). Temperature is estimated from basal heat flow values specified for each time-span event according to the tectonic framework of the NEAG concession, thermal conductivity and surface temperature. The surface temperature trends as a time-latitude diagram (Wygrala 1989) were used to determine SWIT values that depends upon paleo-latitude as well as paleo-water depths (Figure 4). The paleo heat flow values is specified using the known plate tectonic framework and analogies (Allen and Allen 1990, 2005, 2013) adapted for the NEAG concession.

The conceptual model is modified to obtain a better match between simulation outcomes and calibration parameters. The computation of vitrinite reflectance from the well-calibrated temperature histories was carried out using the EASY%Ro algorithm (Sweeney and Burnham 1990). The numerous organic-rich interval in the Khatatba Formation is assigned with the content of organic matter (TOC), hydrogen index (HI) and the specific petroleum generation kinetic parameters. The respective oil-gas kinetic parameters (Pepper and Corvi 1995) have been used for thermogenic hydrocarbon generation (liquid hydrocarbon and gas secondary cracking). The information used for 1D model include formation age, top, thickness, the stratigraphic level for unconformities and associated hiatuses, corrected bottom-hole temperatures, total organic carbon (TOC) content, kerogen type, vitrinite reflectance, Rock-Eval Pyrolysis data and hydrogen indices (HI).

4. Calibration

4.1. Vitrinite reflectance and temperature

The restoration of the burial and thermal histories of the NEAG concession put into action; the basin evolution, basin development, basin-fill sediments and petrophysical properties is accomplished by 1D forward modelling approach. It is critically important to calculate and calibrate the temperature history and predict pore fluid pressures during the evolution of the basin. The compaction state and related porosity facilitated the determination of bulk thermal conductivities for heat flow calculations (Hantschel and Kauerauf 2009). The 1D model was calibrated using vitrinite reflectance (VRr) data obtained from StratoChem Service Company. It constrains the extent of uplift and related erosion as well as provides a calibration of the thermal history. Present-day bottom-hole temperatures, corrected for static formation temperature using Hornet Plot, were used to correct the simulated present-day temperature field. It was necessary to adjust the basal heat flow to attain an agreement between the measured and intended

Table 1. The quantitative chronostratigraphic time-lap conceptual model for the NEAG concession (JD-4 well, see Figure 1 for well location) that belongs to Badr El-Din Petroleum Company (**Bapetco**). The sedimentary sequence is numerically restored by means of well logs data and the available geo-related information. It shows the time-depth relation for the sedimentary section, basin fill history based on the known tectonic framework and crustal evolution of the Gulf of Suez (Figure 2). The facies, successions, ages, source rock properties (TOC, HI, and Kinetics), and reservoir rocks are also represented.

			Thickness		Deposition age		Erosion age		
Name	Top m	Base m	Present m	Eroded m	From Ma	To Ma	From Ma	To Ma	Lithology
Surface	−12	−12	0	0	0.1	0	0	0	Sandstone (typical)
Neogene Deposits	−12	−12	0		1.64	0.1			Sandstone (clay rich)
Kurkar	−12	−12	0	1	3.4	2.3	2.3	1.64	Sandstone (clay rich)
Marmarica	−12	−12	0	1	16.3	6.7	6.7	3.4	Limestone (shaly)
Moghra	−12	468	480	15	26.3	17	17	16.3	Sandstone (clay rich)
Dabaa	468	1115	647		37	26.3			Shale (organic lean, sandy)
Apollonia	1115	1978	863	100	56.5	38.6	38.6	37	Limestone (shaly)
E. Paleocene	1978	1978	0	80	65	57	57	56.5	Shale (organic lean, typical)
Khoman	1978	2680	702	20	84.64	69.1	67.1	65	Limestone (Chalk, typical)
Abu Roash	2680	3109	429	200	93.5	85	85	84.64	Dolomite (typical)
Abu Roash G	3109	3109	0	130	96.2	94.5	94.5	94	Limestone (shaly)
Bahariya	3109	3109	0	240	98.9	96.2	94	93.5	SHALEsand
Kharita	3109	3109	0	960	112.2	99.5	99.5	99	Shale (organic lean, sandy)
Dahab	3109	3109	0	20	115.16	112.2	99	98.95	Shale (organic lean, sandy)
Alamein	3109	3109	0	70	115.66	115.16	98.95	98.9	Limestone (ooid grainstone)
Alam El Buieb	3109	3894	785		119.54	115.66			SANDshaly
Shaltut	3894	3894	0	400	124	120	120	119.77	Sandstone (clay rich)
Betty	3894	3894	0	350	141.8	124	119.77	119.54	Sandstone (clay poor)
Masajid	3894	4162	268	200	164.4	146.36	146.36	141.8	Limestone (shaly)
Upper Safa A1	4162	4311	149		165.86	164.4			Shale (organic lean, typical)
Upper Safa A2-S1[1]	4311	4327	16		166.01	165.86			Shale (organic rich, typical)
Upper Safa A3	4327	4330	3		166.04	166.01			Shale (typical)
Upper Safa A4-S2[2]	4330	4334	4		166.08	166.04			Shale (organic rich, typical)
Upper Safa A5	4334	4340	6		166.14	166.08			Shale (organic lean, sandy)
Upper Safa A6-S3[3]	4340	4342	2		166.16	166.14			Shale (organic rich, 20% TOC)
Upper Safa A7	4342	4351	9		166.25	166.16			Shale (typical)
Upper Safa A8-R1	4351	4353	2		166.27	166.25			Sandstone (typical)
Upper Safa A9	4353	4358	5		166.32	166.27			Shale (organic lean, sandy)
Upper Safa A10-S4[4]	4358	4363	5		166.37	166.32			Shale (organic rich, typical)
Upper Safa A11	4363	4385	22		166.57	166.37			Shale (organic lean, sandy)
Upper Safa A12-R2	4385	4387	2		166.59	166.57			Sandstone (typical)
Upper Safa A13	4387	4412	25		166.83	166.59			Shale (organic lean, sandy)
Upper Safa A14-S5[5]	4412	4415	3		166.86	166.83			Shale (organic rich, typical)
Upper Safa A15	4415	4419	4		166.9	166.86			Shale (organic lean, sandy)
Upper Safa A16-R3	4419	4424	5		166.95	166.9			Sandstone (typical)
Upper Safa A17	4424	4473	49		167.43	166.95			Shale (organic lean, sandy)
Upper Safa B1	4473	4514	41		167.86	167.43			Shale (organic lean, sandy)
Upper Safa B2-R4	4514	4516	2		167.88	167.86			Sandstone (typical)
Upper Safa B3	4516	4567	51		168.39	167.88			Shale (organic lean, sandy)
Upper Safa B4-S6[6]	4567	4569	2		168.41	168.39			Shale (organic rich, typical)
Upper Safa B5	4569	4582	13		168.54	168.41			Shale (typical)
Kabrit1-R5	4582	4591	9		168.58	168.54			Sandstone (typical)
Kabrit2	4591	4659	68		168.9	168.58			SHALE&LIME
Lower Safa A1	4659	4677	18		169.06	168.9			Shale (organic lean, sandy)
Lower Safa A2-S7[7]	4677	4679	2		169.08	169.06			Shale (organic rich, typical)
Lower Safa A3	4679	4764	85		169.83	169.08			SHALEsand
Lower Safa B	4764	4806	42		170.17	169.83			Shale (organic lean, sandy)
Lower Safa C	4806	4908	102		172.84	170.17			SANDshaly
Wadi Natrun	4908	5058	150		180.1	172.84			Shale (organic lean, siliceous, typical)
Bahrein	5058	5258	200		203.8	180.1			Sandstone (clay rich)
Eghei A	5258	5258	0	400	228.9	207	207	205.4	Shale (organic lean, typical)
Eghei B	5258	5258	0	400	245.8	228.9	205.4	203.8	Sandstone (clay rich)
Safi A	5258	5558	300	80	290	250	250	245.8	Limestone (shaly)
Safi B	5558	5908	350	100	332.8	291	291	290	Sandstone (clay rich)
Dhiffah	5908	6008	100	50	339.54	333.8	333.8	332.8	Sandstone (clay poor)
Disouqy	6008	6158	150		358.17	339.54			Sandstone (clay rich)
Zeitoun A	6158	6558	400	200	384.4	361.4	361.4	358.17	Shale (organic lean, sandy)
Zeitoun B	6558	7058	500		402.4	384.4			Sandstone (clay poor)
Basur	7058	7118	60	40	426.14	410.7	410.7	402.4	Sandstone (clay rich)
Kohla	7118	7268	150		439	426.14			Sandstone (clay poor)
Shifah A	7268	7518	250	100	510	441	441	439	Sandstone (clay rich)
Shifah B	7518	7818	300	80	560	512	512	510	Sandstone (clay rich)
Granite	7818	8818	1000		675	600			Granite (500 Ma old)

[1]*Source rock interval with 1.24 wt% TOC, HI is 225 mgHC/g TOC, Kinetics (Pepper and Corvi 1995_TIIS(A)).*
[1]*Source rock interval with 1.24 wt% TOC, HI is 225 mgHC/g TOC, Kinetics (Pepper and Corvi 1995_TIII(H)).*
[2]*Source rock interval with 1.24 wt% TOC, HI is 237 mgHC/g TOC, Kinetics (Pepper and Corvi 1995_TIIS(A)).*
[2]*Source rock interval with 1.24 wt% TOC, HI is 237 mgHC/g TOC, Kinetics (Pepper and Corvi 1995_TIII(H)).*
[3]*Source rock interval with 21.32 wt% TOC, HI is 687 mgHC/g TOC, Kinetics (Pepper and Corvi 1995_TIIS(A)).*
[4]*Source rock interval with 1.69 wt% TOC, HI is 142 mgHC/g TOC, Kinetics (Pepper and Corvi 1995_TIII(H)).*
[5]*Source rock interval with 1.7 wt% TOC, HI is 332 mgHC/g TOC, Kinetics (Pepper and Corvi 1995_TIIS(A)).*
[6]*Source rock interval with 2.21 wt% TOC, HI is 274 mgHC/g TOC, Kinetics (Pepper and Corvi 1995_TIIS(A)).*
[6]*Source rock interval with 2.21 wt% TOC, HI is 274 mgHC/g TOC, Kinetics (Pepper and Corvi 1995_TIII(H)).*
[7]*Source rock interval with 1.2 wt% TOC, HI is 311 mgHC/g TOC, Kinetics (Pepper and Corvi 1995_TIIS(A)).*

temperature data. Vitrinite reflectance and temperature data were available for the JD-4 well, whereas merely temperature data were offered for the JG-2 well (Figure 5). Model predictions are in concordance with measured data (vitrinite reflectance and bottom-hole temperature). The thermal maturity of the Khatatba Formation is inversely affected by the amount of erosion (pre-Safa section 4072m at JG-2

Table 2. The quantitative chronostratigraphic time lap conceptual model for the NEAG concession (JG-2 well) that belongs to Badr El-Din Petroleum Company (**Bapetco**). The sedimentary sequence is numerically restored by means of well logs data and the available geo-related information. It shows the time-depth relation for the sedimentary section, basin fill history based on the known tectonic framework and crustal evolution of the Gulf of Suez. The facies, successions, ages, source rock properties (TOC, HI and kinetics), and reservoir rocks are also represented.

			Thickness		Deposition age		Erosion age		
Name	Top m	Base m	Present m	Eroded m	From Ma	To Ma	From Ma	To Ma	Lithology
Neogene Deposits	−30	−30	0		1.64	0.1			Sandstone (clay rich)
Kurkar	−30	−30	0	1	3.4	2.3	2.3	1.64	Sandstone (clay rich)
Marmarica	−30	−30	0	1	16.3	6.7	6.7	3.4	Limestone (shaly)
Moghra	−30	427	457	20	26.3	17	17	16.3	Sandstone (clay rich)
Dabaa	427	1184	757		37	26.3			Shale (organic lean, sandy)
Apollonia	1184	1884	700	250	56.5	38.6	38.6	37	Limestone (shaly)
E. Paleocene	1884	1884	0	80	65	57	57	56.5	Shale (organic lean, typical)
Khoman	1884	2193	309	400	84.64	69.1	67.1	65	Limestone (Chalk, typical)
Abu Roash	2193	2193	0	650	93.5	85	85	84.64	Limestone (shaly)
Abu Roash G	2193	2193	0	130	96.2	94.5	94.5	94	Limestone (shaly)
Bahariya	2193	2266	73	142	98.9	96.2	94	93.5	SHALEcarb
Kharita	2266	2302	36	930	112.2	99.5	99.5	98.9	Shale (organic lean, sandy)
Dahab	2302	2302	0		115.16	112.2			Shale (organic lean, sandy)
Alamein	2302	2302	0		115.66	115.16			Limestone (ooid grainstone)
Alam El Buieb	2302	2692	390	400	119.54	117.6	117.6	115.66	Shale (organic lean, typical)
Shaltut	2692	2692	0	400	124	120	120	119.77	Sandstone (clay rich)
Betty	2692	2692	0	350	141.8	124	119.77	119.54	Sandstone (clay poor)
Masajid	2692	2834	142	320	164.4	146.36	146.36	141.8	Limestone (shaly)
Upper Safa A1	2834	2903	69		165.24	164.4			Shale (organic lean, sandy)
Upper Safa A2-S1[1]	2903	2905	2		165.33	165.24			Shale (organic rich, 3% TOC)
Upper Safa A3	2905	2908	3		165.37	165.33			Shale (organic lean, sandy)
Upper Safa A4-R1	2908	2922	14		165.55	165.37			Sandstone (typical)
Upper Safa A5	2922	2930	8		165.66	165.55			Shale (organic lean, sandy)
Upper Safa A6-S2[2]	2930	2932	2		165.69	165.66			Shale (organic rich, typical)
Upper Safa A7	2932	2991	59		166.46	165.69			Shale (organic lean, sandy)
Upper Safa A8-S3[3]	2991	2994	3		166.5	166.46			Shale (organic rich, typical)
Upper Safa A9	2994	2998	4		166.55	166.5			Shale (organic lean, sandy)
Upper Safa A10	2998	3040	42		167.1	166.55			Sandstone (clay poor)
Upper Safa A11-S4[4]	3040	3042	2		167.13	167.1			Shale (organic rich, typical)
Upper Safa A12	3042	3048	6		167.21	167.13			SHALE
Upper Safa B1	3048	3052	4		167.26	167.21			SHALEcalc
Upper Safa B2-S5[5]	3052	3054	2		167.29	167.26			Shale (organic rich, typical)
Upper Safa B3	3054	3076	22		167.58	167.29			Shale (organic lean, sandy)
Upper Safa B4-S6[6]	3076	3078	2		167.6	167.58			Shale (organic rich, typical)
Upper Safa B5	3078	3084	6		167.69	167.6			Shale (organic lean, sandy)
Upper Safa B6-S7[7]	3084	3086	2		167.71	167.69			Shale (organic rich, typical)
Upper Safa B7	3086	3100	14		167.89	167.71			Shale (organic lean, sandy)
Upper Safa B8-R2	3100	3104	4		167.94	167.89			Sandstone (typical)
Upper Safa B9	3104	3122	18		168.18	167.94			SHALEcalc
Upper Safa B10-S8[8]	3122	3124	2		168.21	168.18			Shale (organic rich, typical)
Upper Safa B11	3124	3143	19		168.46	168.21			SHALE
Kabrit1	3143	3166	23		168.76	168.46			SHALE&LIME
Kabrit2-S99	3166	3168	2		168.79	168.76			Shale (organic rich, typical)
Kabrit3-R3	3168	3178	10		168.92	168.79			Sandstone (typical)
Lower Safa A1	3178	3184	6		169	168.92			Shale (organic lean, sandy)
Lower Safa A2-R4	3184	3190	6		169.08	169			Sandstone (typical)
Lower Safa A3-S10[10]	3190	3194	4		169.14	169.08			Shale (organic rich, typical)
Lower Safa A4-R5	3194	3218	24		169.45	169.14			Sandstone (typical)
Lower Safa B1	3218	3222	4		169.5	169.45			SHALE
Lower Safa B2-S11[11]	3222	3224	2		169.53	169.5			Shale (organic rich, typical)
Lower Safa B3	3224	3266	42		170.08	169.53			Shale (organic lean, sandy)
Lower Safa C1	3266	3273	7		170.17	170.08			SANDSTONE
Lower Safa C2-S12[12]	3273	3274	1		172.19	170.17			Shale (organic rich, 8% TOC)
Lower Safa C3	3274	3476	202		172.84	172.19			SANDSTONE
Wadi Natrun	3476	3626	150		180.1	172.84			Shale (organic lean, siliceous)
Bahrein	3626	3826	200		203.8	180.1			Sandstone (clay rich)
Eghei A	3826	3826	0	400	228.9	207	207	205.4	Shale (organic lean, typical)
Eghei B	3826	3826	0	400	245.8	228.9	205.4	203.8	Sandstone (clay rich)
Safi A	3826	4126	300	80	290	250	250	245.8	Limestone (shaly)
Safi B	4126	4476	350	100	332.8	291	291	290	Sandstone (clay rich)
Dhiffah	4476	4576	100	50	339.54	333.8	333.8	332.8	Sandstone (clay poor)
Disouqy	4576	4726	150		358.17	339.54			Sandstone (clay rich)
Zeitoun A	4726	5126	400	200	384.4	361.4	361.4	358.17	Shale (organic lean, sandy)

(*Continued*)

Table 2. (Continued).

Name	Top m	Base m	Thickness Present m	Eroded m	Deposition age From Ma	Deposition age To Ma	Erosion age From Ma	Erosion age To Ma	Lithology
Zeitoun B	5126	5626	500		402.4	384.4			Sandstone (clay poor)
Basur	5626	5686	60	40	426.14	410.7	410.7	402.4	Sandstone (clay rich)
Kohla	5686	5836	150		439	426.14			Sandstone (clay poor)

[1]*Source rock interval with 2.61 wt% TOC, HI is 187 mgHC/g TOC, Kinetics (Pepper and Corvi 1995_TIII(H)).*
[2]*Source rock interval with 1.4 wt% TOC, HI is 265 mgHC/g TOC, Kinetics (Pepper and Corvi 1995_TIIS(A)).*
[2]*Source rock interval with 1.4 wt% TOC, HI is 265 mgHC/g TOC, Kinetics (Pepper and Corvi 1995_TIII(H)).*
[3]*Source rock interval with 1.31 wt% TOC, HI is 339 mgHC/g TOC, Kinetics (Pepper and Corvi 1995_TIIS(A)).*
[3]*Source rock interval with 1.31 wt% TOC, HI is 339 mgHC/g TOC, Kinetics (Pepper and Corvi 1995_TIII(H)).*
[4]*Source rock interval with 1.47 wt% TOC, HI is 100 mgHC/g TOC, Kinetics (Pepper and Corvi 1995_TIII(H)).*
[5]*Source rock interval with 2.26 wt% TOC, HI is 294 mgHC/g TOC, Kinetics (Pepper and Corvi 1995_TIIS(A)).*
[5]*Source rock interval with 2.26 wt% TOC, HI is 294 mgHC/g TOC, Kinetics (Pepper and Corvi 1995_TIII(H)).*
[6]*Source rock interval with 1.25 wt% TOC, HI is 172 mgHC/g TOC, Kinetics (Pepper and Corvi 1995_TIII(H)).*
[7]*Source rock interval with 1.74 wt% TOC, HI is 110mgHC/g TOC, Kinetics (Pepper and Corvi 1995_TIII(H)).*
[8]*Source rock interval with 1.5 wt% TOC, HI is 233 mgHC/g TOC, Kinetics (Pepper and Corvi 1995_TIIS(A)).*
[8]*Source rock interval with 1.5 wt% TOC, HI is 233 mgHC/g TOC, Kinetics (Pepper and Corvi 1995_TIII(H)).*
[9]*Source rock interval with 1.02 wt% TOC, HI is 223 mgHC/g TOC, Kinetics (Pepper and Corvi 1995_TIIS(A)).*
[9]*Source rock interval with 1.02 wt% TOC, HI is 223 mgHC/g TOC, Kinetics (Pepper and Corvi 1995_TIII(H)).*
[10]*Source rock interval with 1.67 wt% TOC, HI is 162 mgHC/g TOC, Kinetics (Pepper and Corvi 1995_TIII(H)).*
[11]*Source rock interval with 1.91 wt% TOC, HI is 92 mgHC/g TOC, Kinetics (Pepper and Corvi 1995_TIII(H)).*
[12]*Source rock interval with 9 wt% TOC, HI is 55 mgHC/g TOC, Kinetics (Pepper and Corvi 1995_TIII(H)).*
[12]*Source rock interval with 9 wt% TOC, HI is 55 mgHC/g TOC, Kinetics (Pepper and Corvi 1995_TIIS(A)).*

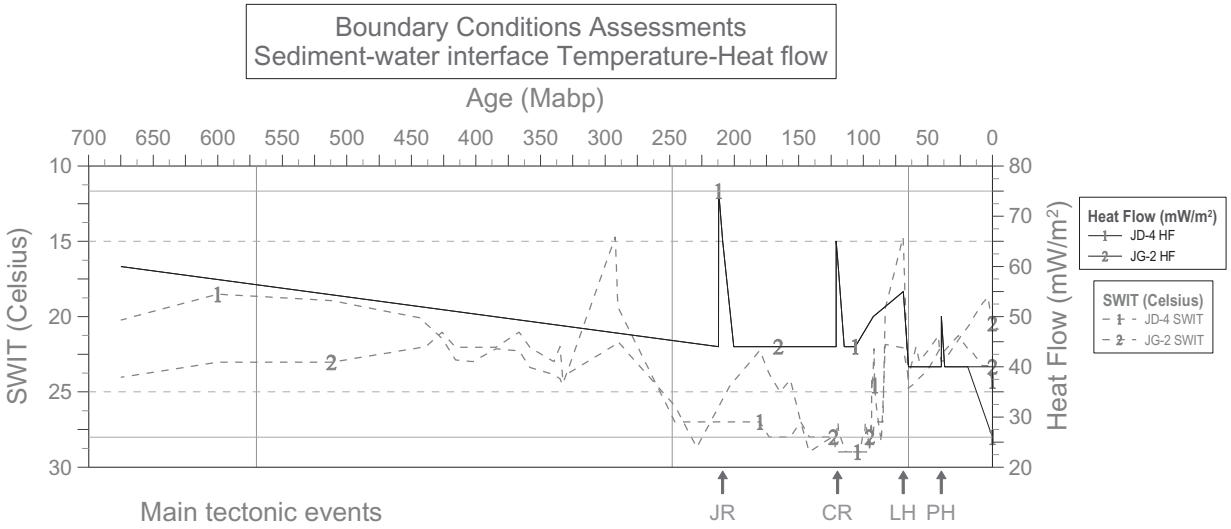

Figure 3. The thermal boundary conditions for JD-4 and JG-2 wells including the sediment-water interface temperature (depends on water depth and paleolatitude, Figure 4) and the paleo-heat flow must be established to determine the interior temperature field. The basal heat flow values were specified for each geologic event using the known plate tectonic framework and crustal evolution models (Allen and Allen 1990). Legend: JR, Jurassic rifting phase (Early Kimmerian); CR, Cretaceous rifting phase (Late Kimmerian); LH, Laramide Hiatus (Syrian Arc System); PH, Pyrenean Hiatus (Inversion Phase). The vertical grid lines represent the era boundaries from left to right: Paleozoic, Mesozoic, and Cenozoic.

well and 2785m at JD-4 well). Consequently, the thermal maturity level is the utmost in the south-eastern part (JD-4 well) where least eroded thickness and thick preserved basin-fill sediments prevailed. Anomalous high thermal maturity level perpendicular to the NE-SW fault system corresponds strongly to a trend of NW-SE thickening of the Khatatba Formation. Temperatures predicted by the well-calibrated 1D model point out a moderate increase with depth (uniform geothermal regime). The predicted low-geothermal gradient at the JD-4 well is in accordance with the rapid sedimentation rate and related low heat flow values. Conversely, the JG-2 well is affected by the hydrocarbon (oil and/or gas) bearing zones (Upper Safa, Kabrit, and Lower Safa). In turns, these has a blanketing effect that led to higher geo-thermal gradients underlain the Lower Safa Member.

5. Results

5.1. Burial history

The burial histories are represented by time-depth plots (Figures 6 and 7) that illustrate the burial of different stratigraphic levels traced throughout geologic time (from deposition to present day). The Middle Jurassic Khatatba sediments were deposited continuously until

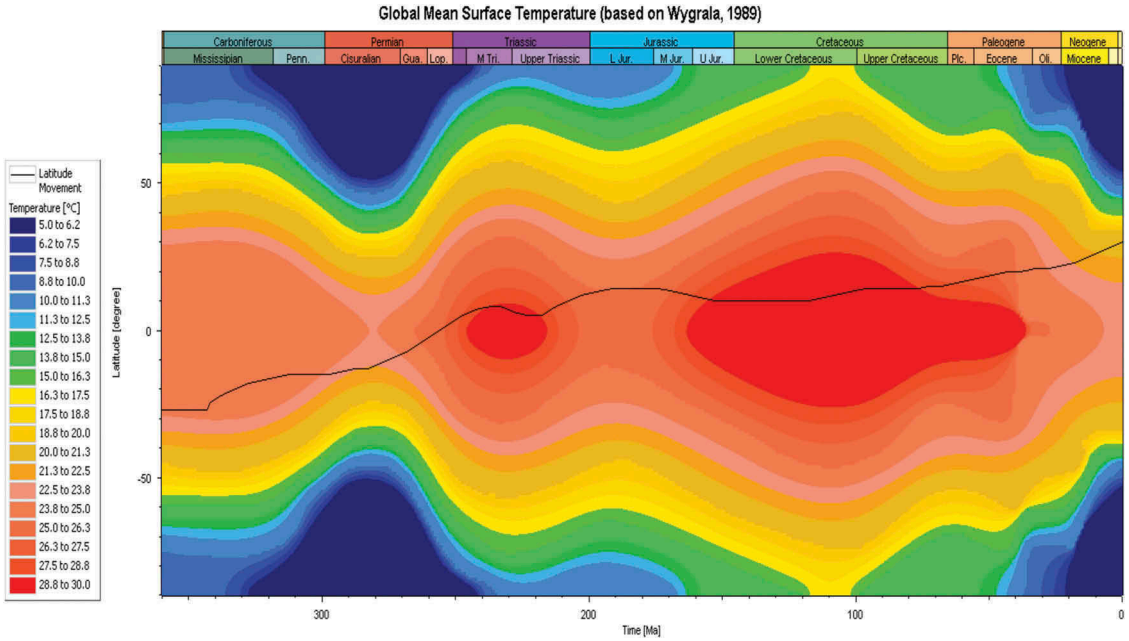

Figure 4. The synthesised sediment–water interface temperature (Wygrala 1989) depends on water depth and paleolatitude. The solid line represents the SWIT of the NEAG concession through geologic time scale and paleolatitude.

a period of uplift occurred in the Late Jurassic–Early Cretaceous (Late Kimmerian Orogeny). Afterwards, renewed subsidence led to the deposition of the Betty and Shaltut sediments (Barremian). The depositional hiatus of the early Aptian (Austrian Unconformity) persisted until a new subsidence commenced that accompanied with the deposition of the Alamein, Dahab and Kharita sediments. Burial history reconstructions of the JG-2 and JD-4 wells show a considerable uplift and erosion that prevailed in the Jurassic, Cretaceous, and Eocene. The burial history charts reflect the availability of greater build-up of basin-fill sediments during the Jurassic. Strata related to basement horst blocks, such as the Kharita Formation experience significant uplift and erosion during the Late Cretaceous at the JG-2 well. The base of the Khatatba Formation attained maximum burial depth of 4908m in JD-4 well at present day, 1432m more than the JG-2 well, where it reached a maximum burial depth of 3476m. Furthermore, erosion related to the Syrian-Arc System removed between 330 and 780m of the Abu Roash sediments at the JD-4 and JG-2 wells, respectively.

5.2. Thermal history

The heat-flux shows a NW-SE variation in the present-day surface heat flow that range from 26 (JD-4 well) to 40 mW/m^2 (JG-2 wells). This trend is almost at right angles to the NE-SW fault plane. In addition, it is in concordance with the thin basin-fill sediments at the JG-2 well and thick basin-fill as well as deep-seated basement at the JD-4 well, respectively. Regular heat flow values of 60 mW/m^2 are assigned as a background value. These values are in concurrence with characteristic heat flow values of post-rift margins that range between 40 and 60 mW/m^2 (Allen and Allen 2013) and common present-day heat flow values in the Abu Gharadig basin. The Cretaceous rifting phase has attained a maximum heat flow value of 75 mW/m^2. The Jurassic rifting phase is set to the heat flow value of 65mW/m^2 that has fewer consequences on the present-day thermal maturity. The Khatatba Formation (Middle Jurassic) was deposited as post-rift basin-fill sediments at shallow depth in younger age. The duration of the rifting phase is relatively short (Jurassic and Cretaceous rifting phases) and a saw tooth-shaped temperature profile is obtained (i.e. an extreme temperature inversion). The Cretaceous rift is rapid compared to the rate of thermal equilibration. This affects thermal maturation by causing significant perturbations in subsurface temperatures as illustrated in Figure 8. Chalk of the Khoman Formation, the shaley limestone of the Masajid Formation, the shale intervals as well as the multiple organic-rich intervals of the Khatatba Formation (Safa members) are of relatively low thermal conductivity. Therefore, the underlying sediments will be warmer (the so-called a Blanketing Effect). This led to a high geothermal gradient with low temperature at the top and high at the bottom.

5.3. Organic geochemistry

The Khatatba samples (46 cores and cuttings) have Total Organic Carbon (TOC) varying from 1.02 to 9.09 wt.% with an average 2.11wt.% and hydrogen index (HI) in the range of 55–687 mgHC/g TOC (Tables 3 and 4). Only one sample from the JD-4 well (Upper Safa A-S3) at a depth interval of 4340-4342m

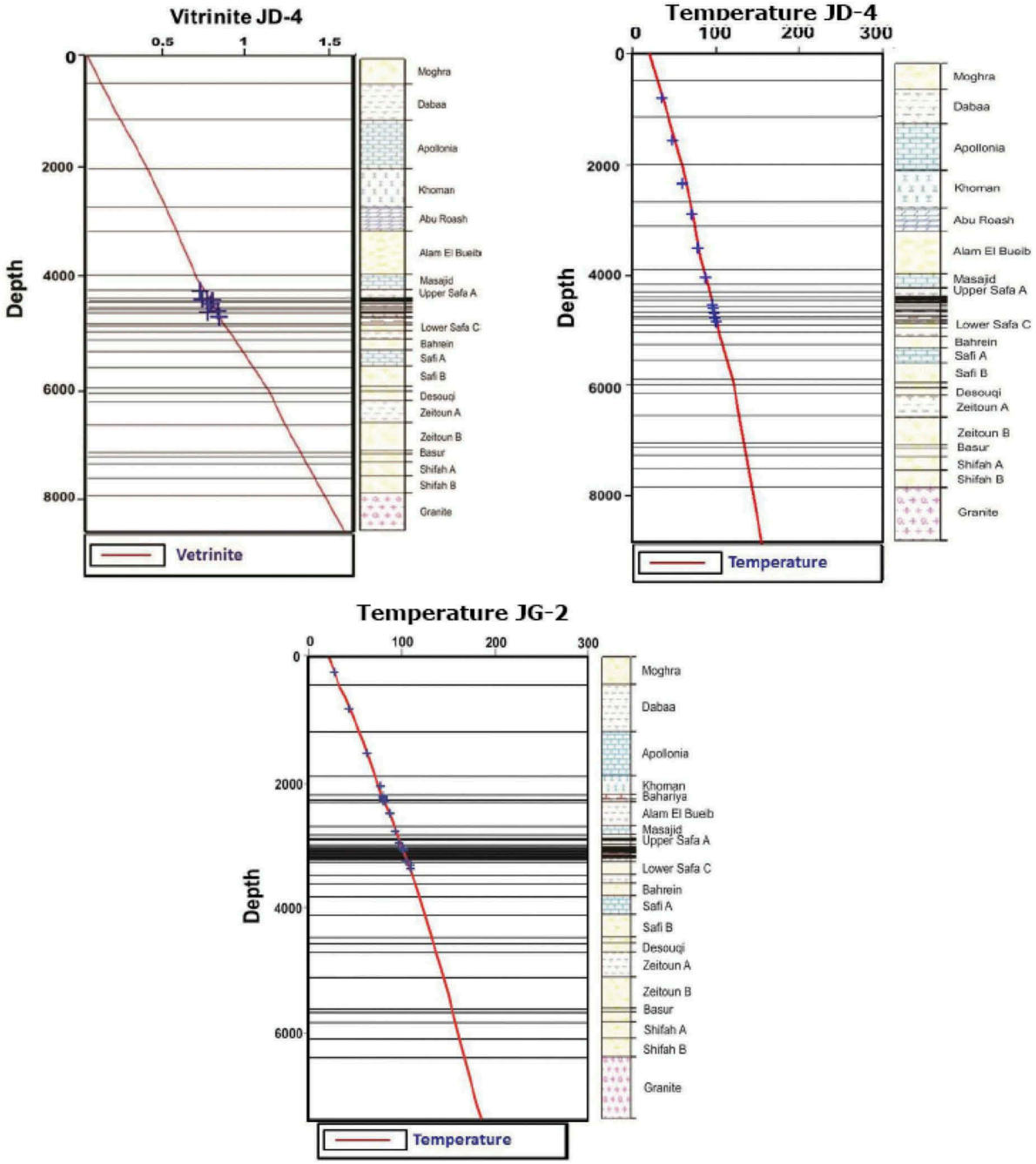

Figure 5. One-dimensional model extractions at selected well locations showing the best fit of the modelled (line) and measured (plus sign) vitrinite reflectance data (JD-4 well) as well as temperature profile (JD-4 and JG-2 wells). The plot of paleotemperature is calibrated with corrected static bottom-hole temperature in reference wells.

TVDss has anomalous TOC value of 21.32wt%. The relatively high HI (687mgHC/gTOC) and low OI (4 $mgCO_2$/gTOC) pinpoint that the kerogen comprises oxygen-lean organic-rich materials. This verifies a type II kerogen with an oil generating potential. T_{max} values range from 410 to 449°C with an average value of 439°C and the mean vitrinite reflectance is 0.85%Ro. Additionally, Rock-Eval Pyrolysis data indicate the presence of three kerogen types within the Khatatba Formation (II, III and II/III) and the latter type is the most dominant (Figures 9 and 10). These organic-rich intervals are oil and/or gas prone in addition to oil and (or) gas generation potential.

The analysed samples retrieved from 19 organic-rich intervals from two wells; seven recognised within the JD-4 Khatatba sub-units and 12 in the JG-2 well. Such intervals generally exhibit an excellent generating potential for liquid hydrocarbons (oil prone type II kerogen), gas (gas prone type III kerogen) and oil/gas (oil/gas prone type II/III kerogen).

5.4. Thermal maturity and hydrocarbon generation

The depth of the Middle Jurassic Khatatba Formation ranges from 2834 m at JG-2 well to 4162 m TVDss at JD-

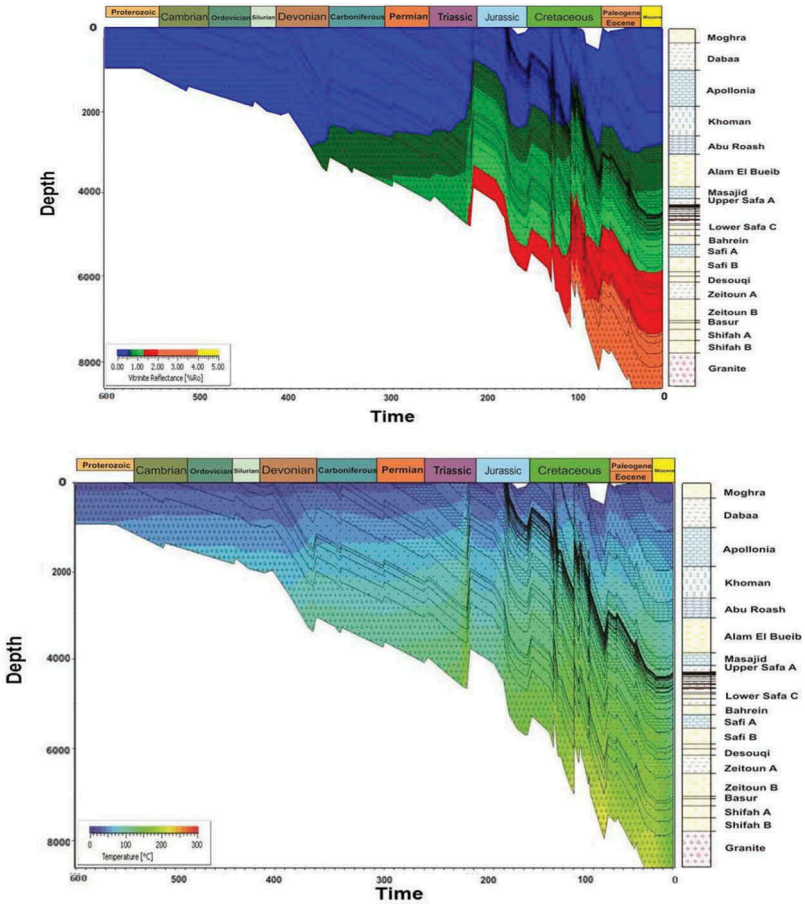

Figure 6. (a) The simulated vitrinite reflectance value and the associated geohistory of all formations in a reference well (JD-4) against time (Ma) and depth (m). The calculated vitrinite reflectance value carried out using the Easy %Ro algorithm (Sweeney and Burnham 1990) against geologic time scale (Ma). (b) Quantitative simulated geohistory, burial history and recalibrated temperature development history as a function of time and space of the reference JD-4 well. The solid lines traces the depth-time relation for the sediment with discrepancy between present (compacted) and decompacted thickness. The lower curve shows subsidence of the basement. The upper curves are the sediment interface.

4 well. The penetrated thickness varies from 638 m to 746 m at JG-2 well and JD-4 well, respectively. It deposited in a markedly anoxic outer shelf environment and composed of marginal marine shale (Palmer 1993). The organofacies reached the main stage of oil generation in the Early Cretaceous at the JD-4 well (Figure 11). However, the peak oil generation at the JG-2 well was attained later (102 Ma ago) after the deposition of the Kharita Formation. The organic-rich intervals (oil prone type II kerogen) entered the oil window at JD-4 well close to the Albian (~108.59 Ma) and the wet gas window since late Albian (~105.35 Ma). This is accompanied the deposition of the Kharita Formation and subsequent to the Early Cretaceous Rifting Phase and its related thermal subsidence. In contrast, the Khatatba organofacies (gas prone type III kerogen) reached the dry-gas window since ~30.91 Ma (early Oligocene) at the JD-4 well, prior to the wet-gas window of the JG-2 well (~26.3 Ma late Oligocene), contemporaneous to the deposition of the Dabaa Formation (Figure 12). Nevertheless, the Khatatba organic-rich interval (gas prone type III kerogen) never attained the dry gas window at JG-2 well due to its low thermal maturation level.

The present-day simulated vitrinite reflectance (Sweeney and Burnham 1990) values alongside the present-day depth show different Ro% values for the organic-rich intervals (S1-S7) at JD-4 well and (S1–S12) at JG-2 well. The shallower basement relief well explains the utmost present-day temperature of 106°C at JG-2. Moreover, the consequence of the totally missed sediments of the Abu Roash Formation (780 m) plus the low thickness of Masajid (142 m), Alam El Buieb (390 m) and Khoman (309 m) formations. At JD-4 well low thermal conductivity sediments of (268 m) for Masajid, (785 m) for Alam EL Bueib and (702 m) for Khoman formations have been deposited. Nevertheless, the present-day maximum simulated Ro value of 0.9% at the JD-4 well corresponds to a temperature value of 99°C. This is due to the burial effect attributable to the great thicknesses of the Masajid, Alam El Bueib, Abu Roash and Khoman sediments. In contrast, the present-day minimum simulated Ro value of 0.65% and a temperature value of 97°C have been obtained at the JG-2 well for the Upper Safa A-S1. This is explained by the little thickness of shale in the Kharita Formation (36m) as well as the low thickness of

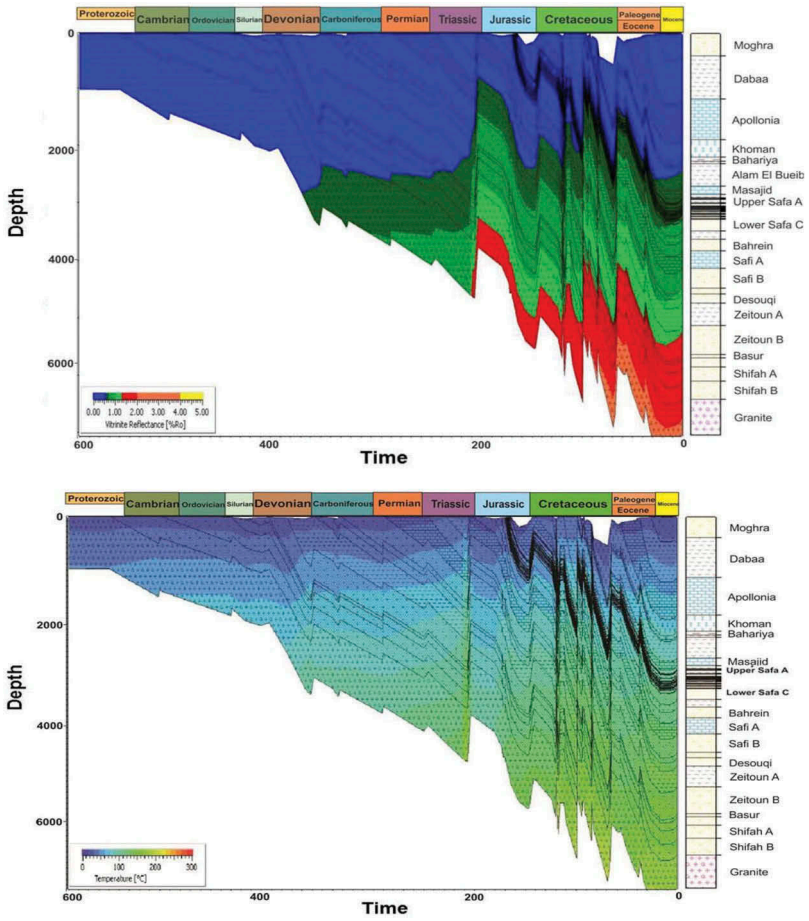

Figure 7. (a) The simulated vitrinite reflectance value and the associated geohistory of all formations in a reference well (JG-2) against time (Ma) and depth (m). The calculated vitrinite reflectance value carried out using the Easy %Ro algorithm (Sweeney and Burnham 1990) against geologic time scale (Ma). (b) Quantitative simulated geohistory, burial history and recalibrated temperature development history as a function of time and space of the reference JG-2 well. The solid lines traces the depth-time relation for the sediment with discrepancy between present (compacted) and decompacted thickness. The lower curve shows subsidence of the basement. The upper curves are the sediment interface.

the chalk deposits in the Khoman Formation (309m). These sediments are characterised by relatively low thermal conductivity that effectively reduces the vertical heat transfer. In turns, explains the absence of any suggested mature younger organic-rich intervals. The low thickness decreases the capability of heat retention necessary for thermal maturation. For that reason, the thermal maturity at the JG-2 well is related to the basin evolution and development with a modest influence of burial. The oil window is shallower in depth at the JD-4 well compared to that at the JG-2 well. However, the gas generation depth ranges from 2439 m (~105.35 Ma Cretaceous) to 2838 m (~27.41 Ma Oligocene) at the JD-4 and JG-2 wells, respectively.

5.5. Transformation ratio

The present-day transformation ratio ranges from 21% at JG-2 well to 89% at the JD-4 well whereas the maximum bulk generation mass is 0.46 Mtons obtained at present-day in the JD-4 well (Figures 13 and 14). At the JD-4 well, an abrupt increase in the transformation ratio has obtained at ~28.52 Ma (Oligocene) owing to increased heating rate that accompanied the Inversion Phase.

5.6. Expulsion and migration

Hydrocarbon expulsion began in the southeast part (JD-4 well) during the Late Cretaceous to Oligocene. Oil expulsion from the Upper Safa A-S3 occurred during the Miocene-Tertiary in the northwest part (JG-2 well). The oil expulsion commenced from the Lower Safa A-S7 since Late Cretaceous at the JD-4 well, while gas expulsion occurred from the Upper Safa B-S6 in Oligocene. The expulsion onset occurred in Late Cretaceous (~82.91 Ma) at depth 2849 m (TVDss) in JD-4 well, in contrary to JG-2 well, whereas it started in the Miocene (~7.7 Ma) at depth 3096 m. The oil prone type II kerogen (S3, S5 and S7) as well as oil and (or) gas prone type II/III kerogen (S1, S2, S4 and S6) in the JD-4 well expelled oil since Late Cretaceous (~82.91 Ma) during the deposition of the Khoman Formation. The Upper Safa B-S6 interval (mixed oil and gas character) initiated gas expulsion during the deposition of the Oligocene Moghra

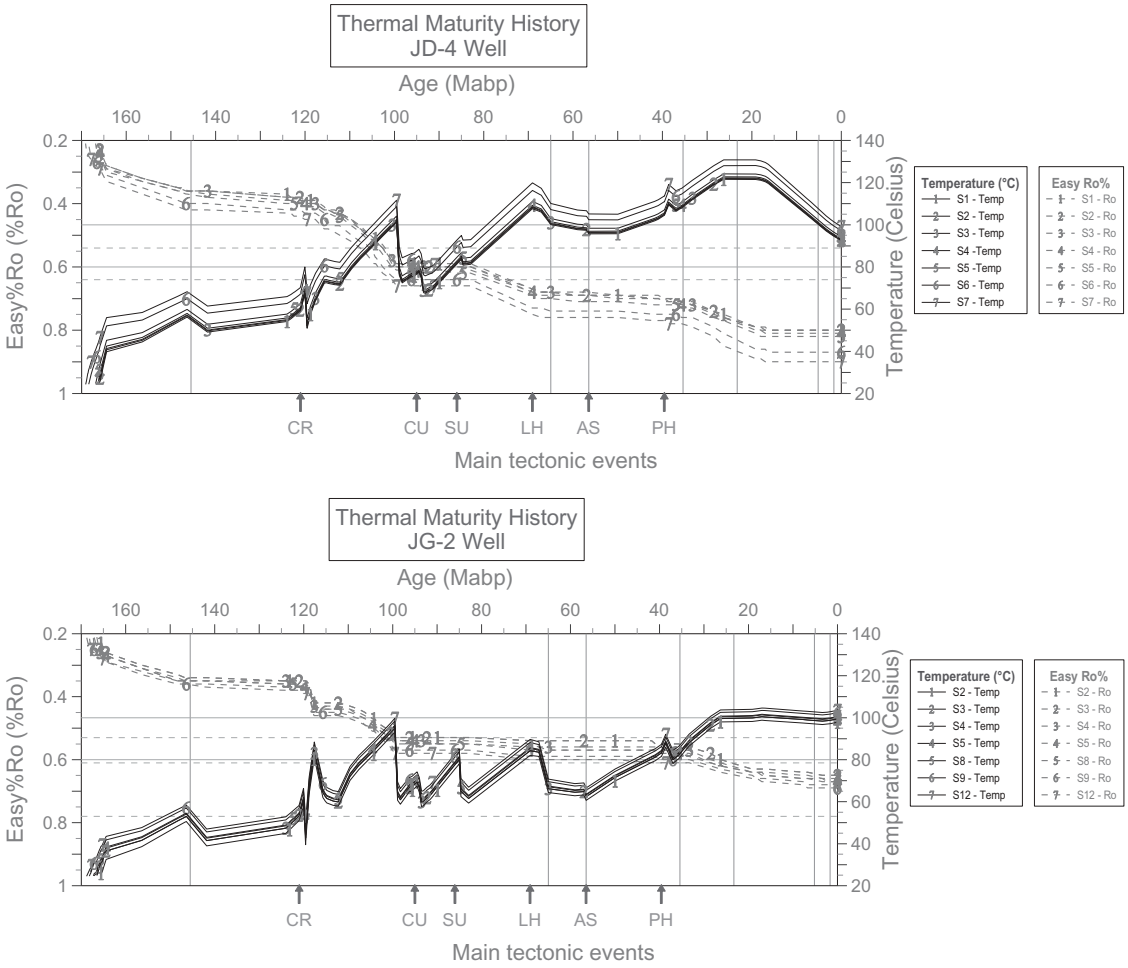

Figure 8. The simulated vitrinite reflectance value and the associated thermal history of the Khatatba organic-rich intervals at in the JD-4 well (upper) and the JG-2 well (lower). The calculated vitrinite reflectance value carried out using the EASY%Ro algorithm (Sweeney and Burnham 1990) plus temperature profile plotted against geologic time scale (Ma) with zoon in form the Cretaceous to Recent time. Legend: CR, Cretaceous Rifting phase; CU, Cenomanian unconformity; SU, Santonian unconformity; LH, Laramide Hiatus (Syrian Arc System); AS, Active subsidence; PH, Pyrenean Hiatus (Inversion Phase). The vertical grid lines represent the age boundaries from left to right: Cretaceous, Paleocene, Eocene, Oligocene, Miocene, Pliocene and recent.

Table 3. Jurassic Khatatba Formation organofacies intervals and its properties used for 1D modelling and simulation of hydrocarbon generation in the NEAG Concession, JD-4 well, Abu Gharadig basin–Western Desert.

TVDSS	Kerogen	S1	S2	TOC	Easy%Ro	HI	OI	T_{max}	h	Member	Zone Name
4311	II/III	0.13	2.79	1.24		225	56	445	16	Upper Safa	A2-S1
4330	II/III	0.4	2.94	1.24		237	37	445	4	Upper Safa	A4-S2
4340	II	0.47	146.5	21.32		687	4	445	2	Upper Safa	A6-S3
4358	III	0.1	2.4	1.69	0.85	142	28	445	5	Upper Safa	A10-S4
4412	II	0.17	5.64	1.7		332	42	445	3	Upper Safa	A14-S5
4567	II/III	0.17	6.05	2.21	0.9	274	19	448	2	Upper Safa	B4-S6
4677	II	0.16	3.73	1.2	0.92	311	40	449	2	Lower Safa	A2-S7

TVDSS: True vertical depth sub-sea level; S1:mg/g; S2:mg/g; TOC: Total organic carbon (wt%); EASY%Ro: Calculated vitrinite reflectance using (Sweeney and Burnham 1990) (%); HI: Hydrogen Index (mgHC/gTOC); OI: Oxygen Index (mgCO2/gTOC); Tmax:degC and h: The true thickness (meter).

Formation (~26.3 Ma) at depth 4449 m. However, the gas prone type II kerogen (S1, S4, S6, S7, S10 and S11) and oil/gas prone type II/III kerogen (S2, S3, S5, S8, S9 and S12) exhibited neither thermogenic gas generation nor gas secondary cracking at the JG-2 well and expect no expulsion. The efficiency of expulsion depends on the petrophysical properties of the source rock (Littke and Leythaeuser 1993). The resulted low expulsion efficiency causes a preservation of hydrocarbon until gas is generated by cracking of the trapped bitumen at more elevated maturity. The expelled hydrocarbons (oil and/or gas) from the mature/effective Khatatba organofacies at the JD-4 well may be migrated laterally upward (northwestward to the JG-2 well) through the NE-SW Jurassic fault plane.

6. Discussion

Despite the thermal maturity of the Khatatba organofacies has been assigned to the oil window (El Diasty

Table 4. Jurassic Khatatba Formation organofacies intervals and its properties used for 1D modelling and simulation of hydrocarbon generation in the NEAG Concession, JG-2 well, Abu Gharadig basin–Western Desert.

TVDSS	Kerogen	S1	S2	TOC	HI	OI	T_{max}	h	Member	Zone Name
2903	III	0.51	4.89	2.61	187	34	436	2	Upper Safa	A2-S1
2930	II/III	0.48	3.71	1.4	265	39	432	2	Upper Safa	A6-S2
2991	II/III	2.34	4.55	1.31	339	34	436	3	Upper Safa	A8-S3
3040	III	0.5	1.47	1.47	100	28	433	2	Upper Safa	A11-S4
3052	II/III	0.58	6.64	2.26	294	31	433	2	Upper Safa	B2-S5
3076	III	0.56	2.15	1.25	172	44	432	2	Upper Safa	B4-S6
3084	III	0.48	1.62	1.47	110	39	433	2	Upper Safa	B6-S7
3122	II/III	0.65	3.5	1.5	233	35	434	2	Upper Safa	B10-S8
3166	II/III	0.72	2.27	1.02	223	57	432	2	Kabrit	2-S9
3190	III	1.2	2.73	1.67	163	26	430	4	Lower Safa	A3-S10
3222	III	0.33	1.75	1.91	92	28	433	2	Lower Safa	B2-S11
3273	II/III	5.63	4.99	9	55	3	432	1	Lower Safa	C2-S12

TVDSS: True vertical depth sub-sea level; S1:mg/g; S2:mg/g; TOC: Total organic carbon (wt%); EASY%Ro: Calculated vitrinite reflectance using (Sweeney and Burnham 1990) (%); HI: Hydrogen Index (mgHC/gTOC); OI: Oxygen Index (mgCO2/gTOC); Tmax:degC and h: The true thickness (meter).

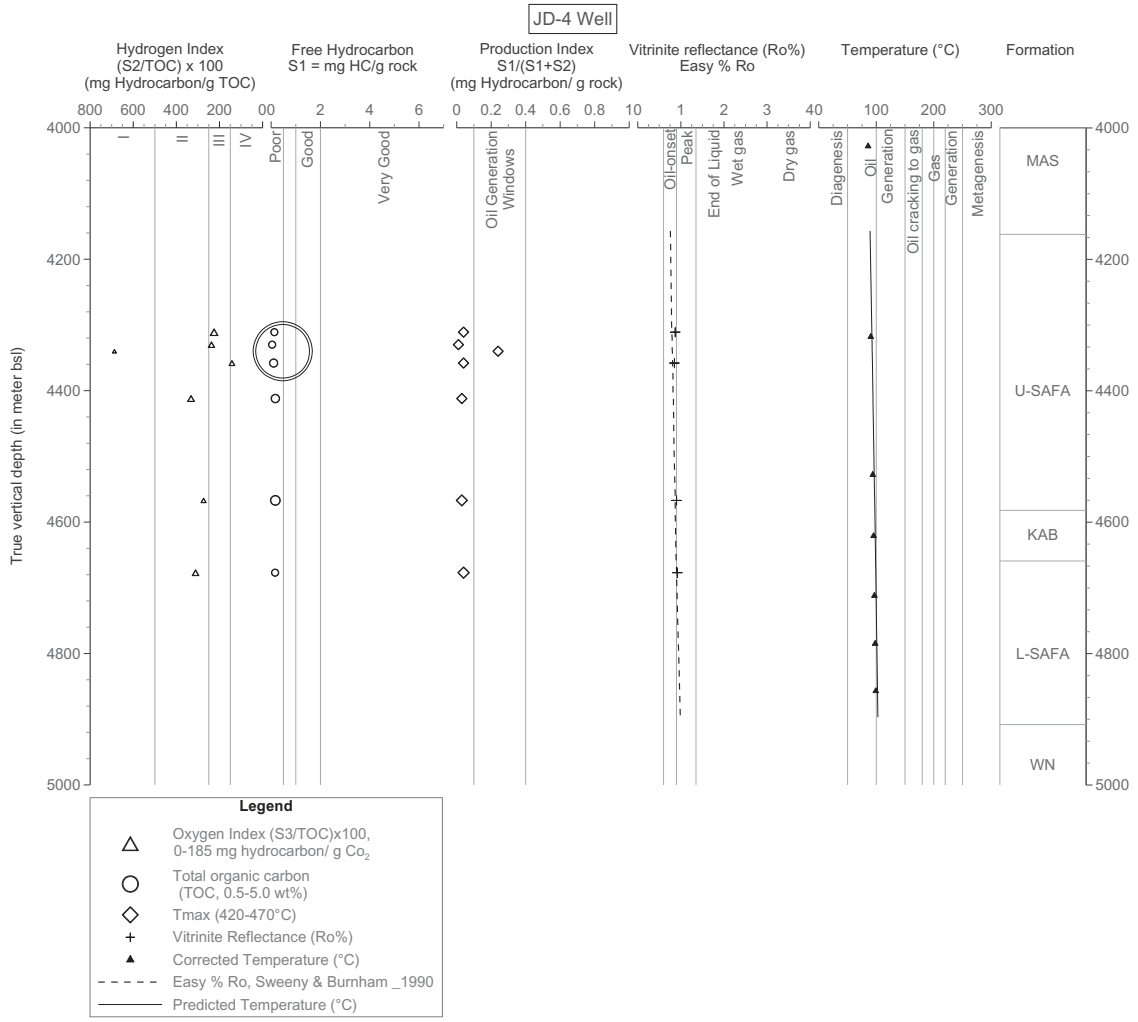

Figure 9. Idealised geochemical log based on Rock-Eval Pyrolysis, total organic carbon (TOC) and vitrinite reflectance samples from a reference well-JD-4 shows a evidence for thermally mature (active) source rock containing type II-S, III and II/III kerogen. Vitrinite reflectance-depth plot showing the generalised position of the oil and gas zones, which will vary depending on kerogen type. These Ro% values are related to the maximum temperature to which a particular zone has been exposed. MAS: Masajid Formation; U-SAFA: Upper Safa Member; KAB: Kabrit Member; L-SAFA: Lower Safa Member and WN: Wadi Natrun Formation.

2015), the thermal maturity history, timing of hydrocarbon generation, the probability of gas generation (either primary cracking (gas prone type III kerogen) or secondary generation (oil prone type II kerogen)) and the consequential expulsion have never been discussed. The results obtained from the 1D-model redresses such imbalance, with respect to basin development, tectonic framework, burial and basin-fill history of Abu Gharadig basin. The petroleum system elements hereby are investigated based on petrophysical evaluation either as a fundamental tool (defining reservoir intervals and the type of hydrocarbon

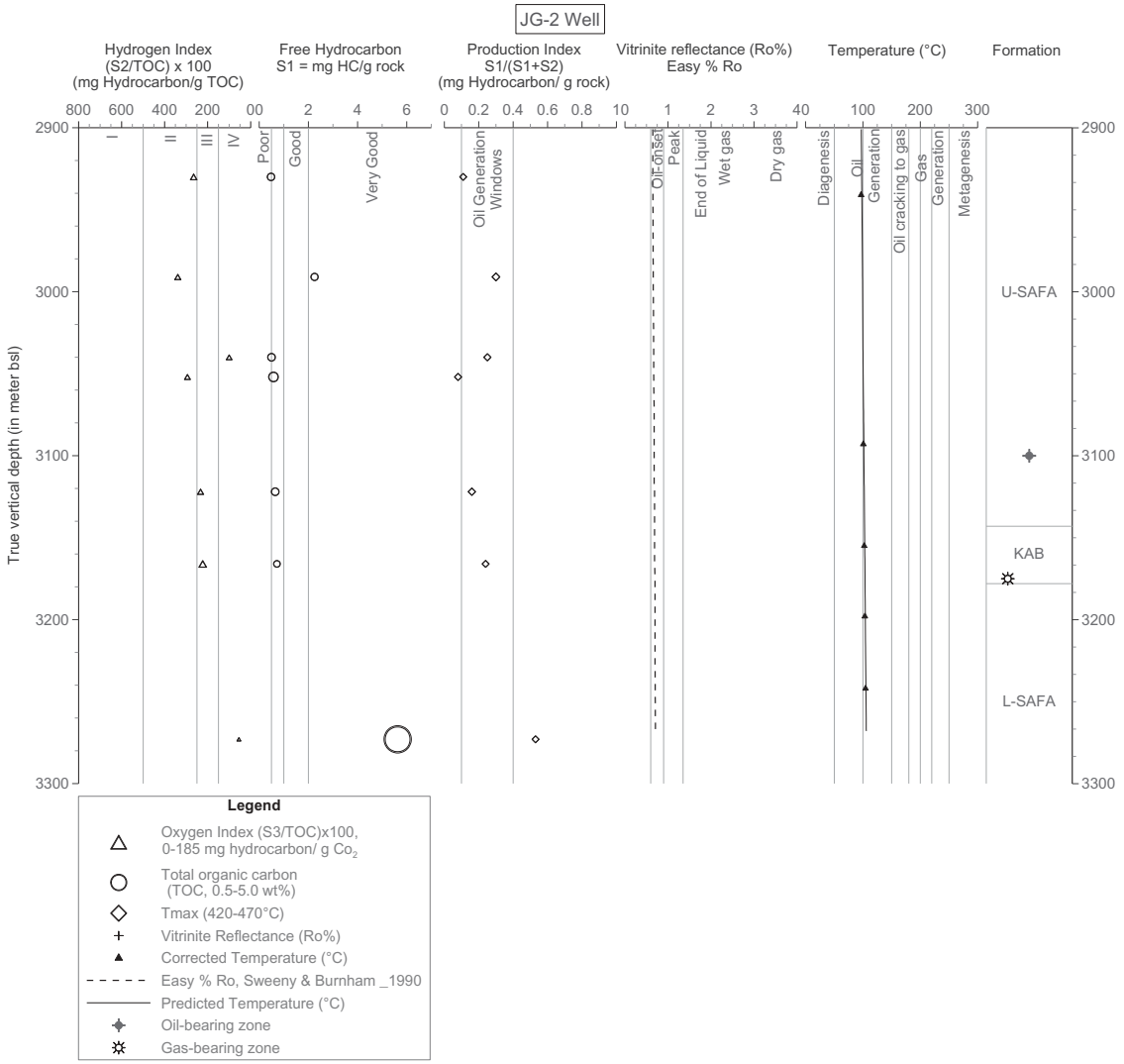

Figure 10. Idealised geochemical log based on Rock-Eval Pyrolysis and total organic carbon (TOC) from a reference well-JG-2 shows a evidence for (a) thermally immature (potential) source rock containing type III kerogen, (b) mature source rock containing type II-S and/or III kerogen, and (c) reservoir rock. Vitrinite reflectance-depth plot showing the generalised position of the oil and gas zones, which will vary depending on kerogen type. These Ro% values are related to the maximum temperature to which a particular zone has been exposed. MAS: Masajid Formation; U-SAFA: Upper Safa Member; KAB: Kabrit Member; L-SAFA: Lower Safa Member and WN: Wadi Natrun Formation.

accumulated) or a supplementary tool to the conventional organic geochemistry (qualitative source rock analysis (recognition and thermal maturity determination)).

1D model outcomes point out that the gas prone type III kerogen of JG-2 well are generally immature despite their stratigraphic position. Maturation histories propose that the lower part of the Khatatba Formation became locally mature during the Early Cretaceous (JD-4 well). The composition of the generated hydrocarbons varies relative to the level of thermal maturities and type of kerogen. This was supported by the conclusion that oil has been originated from terrigenous-dominated marine source rocks or mixed terrigenous marine organic matter (El Diasty 2015). However, a general southeastward (JD-4 well) increase in thermal maturity is accompanied by a raise in gas wetness and high flux due to burial.

The oil window is older (108.59 Ma) at JD-4 well as well as shallower than that at the JG-2 well. The last is influenced by the deposition of thick (36 m) shaley sediments of Kharita Formation and Dabaa sediments 389 m. Additionally the Abu Roash Formation is completely eroded at JG-2 well. The Khatatba organofacies entered the oil window since Late Cretaceous (Campanian-Maastrichtian ~75.99 Ma) at the JG-2 well following the Late Cretaceous Rifting Phase (~93.5–95 Ma), the Syrian Arc System (~84.64–86 Ma) and throughout the deposition of the Khoman Formation. This confutes the onset of oil maturation in the JG-2 well to late Oligocene (~27.2 Ma) (Maky and Ramadan 2008). Consequently raises uncertainties concerning the Time Temperature Index (TTI) as an efficient tool for predicting the accurate timing of oil window. The generated hydrocarbon at the JD-4 well is in the phase of oil and gas while liquid phase only is

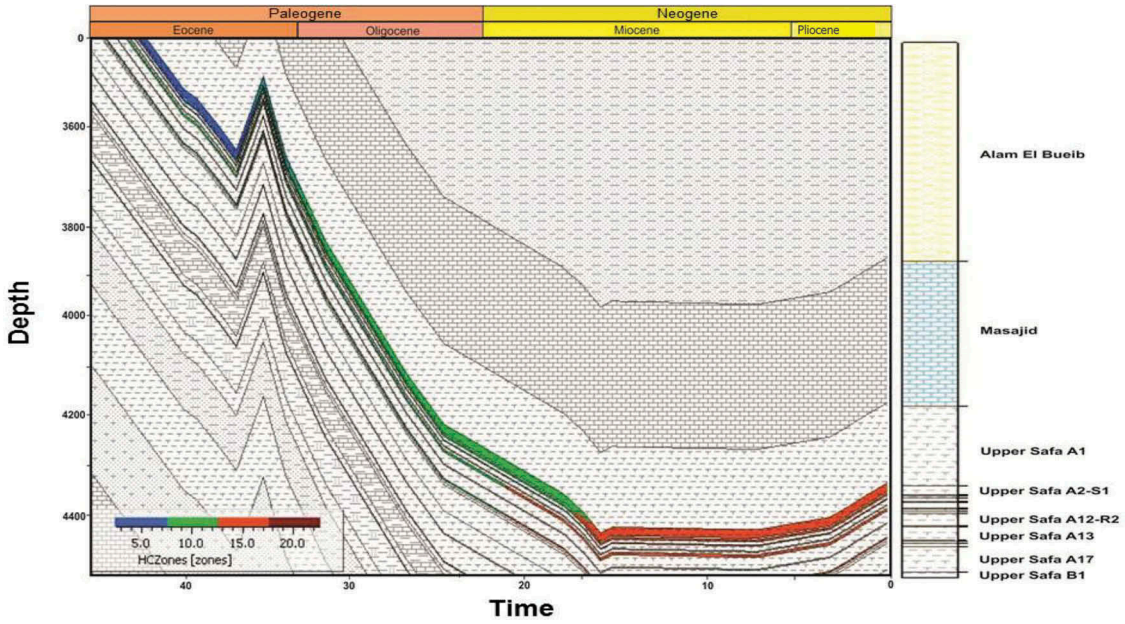

Figure 11. The simulated burial history at JD-4 well with the hydrocarbon zone properties overlay according to the Pepper&Corvi 1995_TIIS(A) oil-gas kinetics equation (Pepper and Corvi 1995) for the source interval of the Khatatba Formation through geologic time scale (Ma).

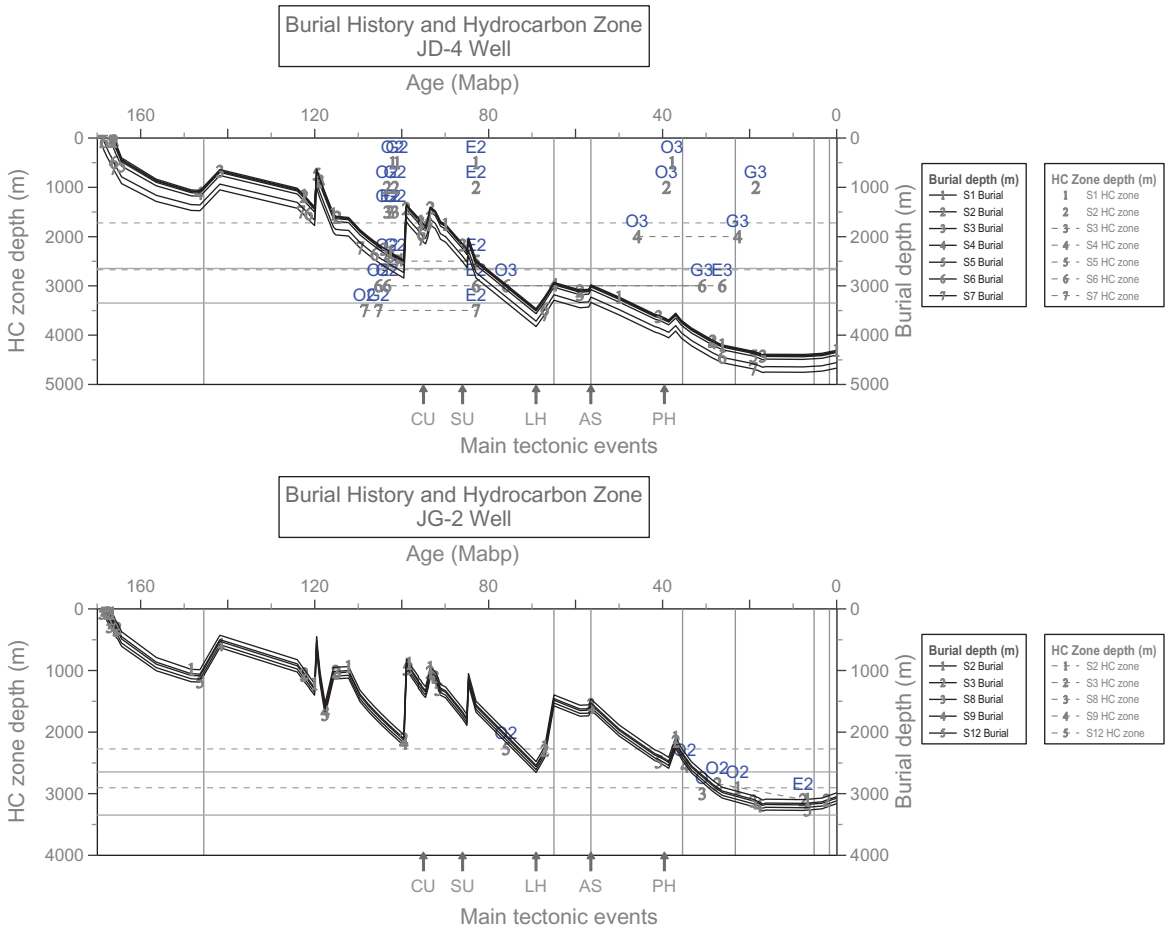

Figure 12. The simulated burial history of the Khatatba Formation organofacies at JD-4 well (upper) and JG-2 well (lower), with the hydrocarbon zone properties overlay according to the oil-gas kinetics equation of (Pepper and Corvi) through geologic time scale (Ma). Legend: CU, Cenomanian unconformity; SU, Santonian unconformity; LH, Laramide Hiatus (Syrian Arc System); AS, Active subsidence; PH, Pyrenean Hiatus (Inversion Phase). The vertical grid lines represent the age boundaries from left to right: Cretaceous; Paleocene; Eocene; Oligocene; Miocene; Pliocene; and recent; O, Oil window depth; G, Gas window depth; E, Expulsion window depth; 2, Kerogen type II/II-S and 3, Kerogen type III. The simulated burial history of Khatatba Organic-rich interval with the hydrocarbon zone properties overlay according to the oil-gas kinetics equation of through geologic time scale (Ma) (a) in the JD-4 well, (b) in the JG-2 well.

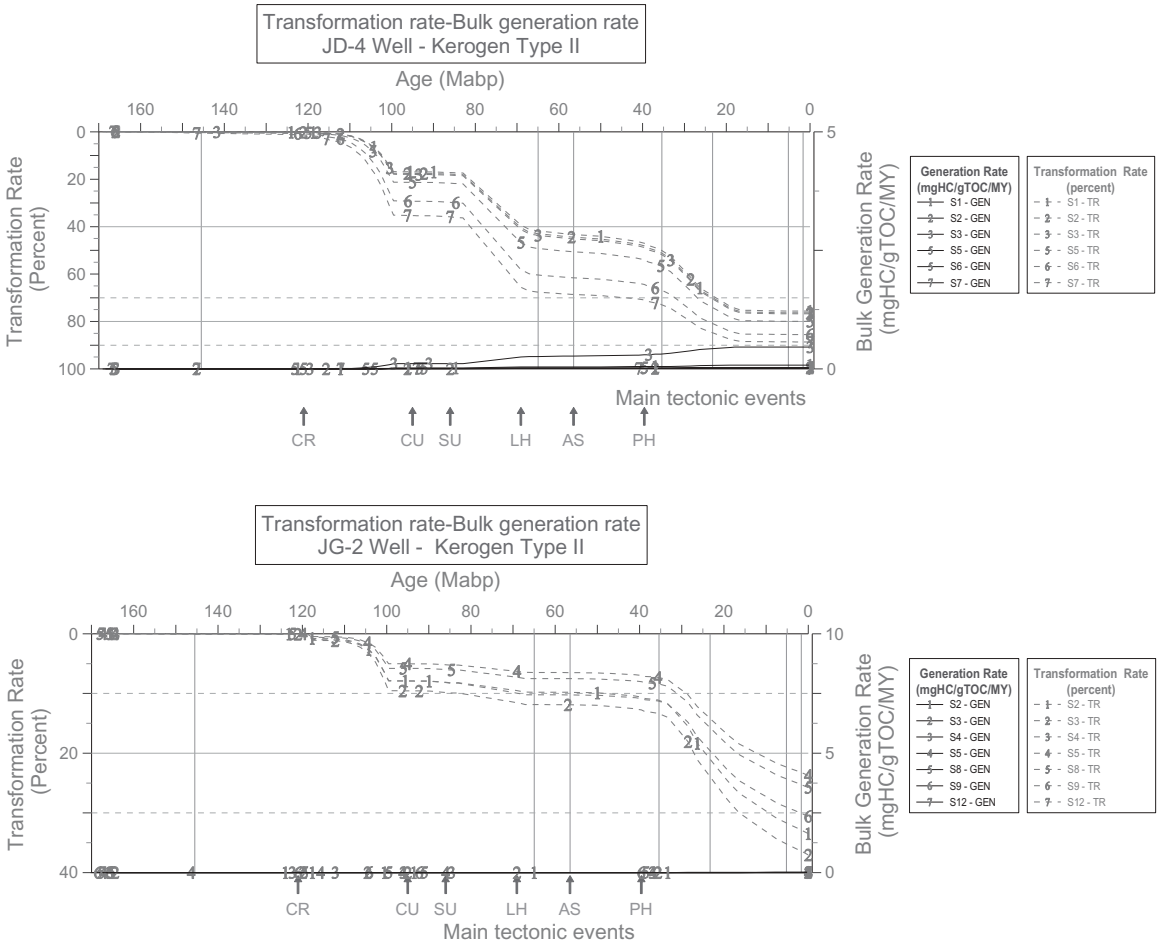

Figure 13. Plot of the formation transformation ratio (percent) and the bulk generation rate (mgHC/gTOC/MY) for Jurassic Khatatba Formation organofacies (Kerogen Type II) in the reference wells JD-4 (upper) and JG-2 (lower) against geologic time scale (Ma). Legend: CR, Cretaceous rifting phase (Late Kimmerian); CU, Cenomanian unconformity; SU, Santonian unconformity; LH, Laramide Hiatus (Syrian Arc System); AS, Active subsidence; PH, Pyrenean Hiatus (Inversion Phase). The vertical grid lines represent the age boundaries from left to right: Cretaceous, Paleocene, Eocene, Oligocene, Miocene, Pliocene and recent.

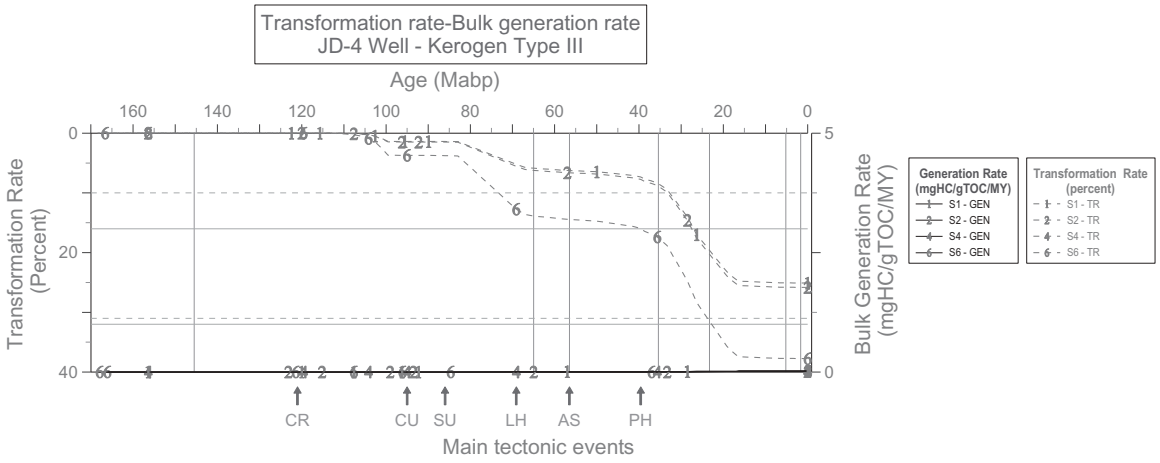

Figure 14. Plot or the transformation ratio (percent) and the bulk generation rate (mgHC/gTOC/MY) for Jurassic Khatatba Formation organofacies (Kerogen Type III) in a reference well (JD-4) against geologic time scale (Ma). Legend: CR, Cretaceous rifting phase (Late Kimmerian); CU, Cenomanian unconformity; SU, Santonian unconformity; LH, Laramide Hiatus (Syrian Arc System); AS, Active subsidence; PH, Pyrenean Hiatus (Inversion Phase). The vertical grid lines represent the age boundaries from left to right: Cretaceous, Paleocene, Eocene, Oligocene, Miocene, Pliocene and recent.

prevailing at the JG-2 well. The thick basin-fill sediments (overburden) that superimpose the Khatatba Formation plus the deep-seated basement at the JD-4 well accelerated the hydrocarbon generation compared to the JG-2 well. The improved burial effect in the JD-4 well was influenced by the deposition of the thick succession of the Masajid (268 m), Alam El Bueib (785 m), Abu Roash (429 m) and Khoman (702 m) formations.

In additions, drawbacks in the use of vitrinite reflectance measurements (Heroux et al. 1979; Kubler et al. 1979; Durand et al. 1986) taken from maceral types other than vitrinite (Bensley and Crelling 1994) frequently results in apparent suppression of reflectivity of the vitrinite (Price and Barker 1985). Other drawbacks are the possibility of reworking of organic material and the lack of higher plants yielding vitrinite in pre-Devonian strata. Accordingly, vitrinite reflectance tends to be unreliable at low levels of thermal maturity (Ro less than 0.7 or 0.8%). Whereas, at high temperatures equivalent to depths of>4 km the vitrinite maceral is increasingly anisotropic, making accurate measurement problematical. Nevertheless, reflectance values are a good indicator of maximum paleo-temperature within the approximate depth range of 1–4 km (Whelan and Thomson Rizer 1993).

The majority of the oil in the NEAG concession is of high sulphur content and originated from a marine shale Middle Jurassic Khatatba source rock (El Diasty 2015). The model illustrates two general trends of increased thickness (Khatatba Formation) that is unrelated to present-day basin geometry and axis but to a certain extent associated with structural elements such as Jurassic fault system. One of these trends encircles at the JD-4 well (a southeast trend perpendicular to the NE-SW Jurassic fault system). While the other surrounds the JG-2 well. The SE trend is coincident with increased thermal maturities of the Khatatba organic-rich intervals, as indicated by mean vitrinite reflectance values (Ro = 0.85%). These faults acted as conduits for migration where hydrocarbon accumulated in potential reservoirs (Khatatba Formation) of the northwest traps. A 2D model is supposed to validate this further. It is expected that migration of the expelled thermogenic gas into the uplifted area occurred in the Miocene.

7. Conclusions

Integrated 1D basin modelling was applied to assign the thermal-maturation, hydrocarbon generating-potential and expulsion of the multiple organic-rich intervals and its influence on hydrocarbon potentiality in the NEAG concession. Best concordance between measured and calculated present-day temperatures and vitrinite reflectance was achieved with present-day heat flows in the range of 26-40 mW/m^2. The scenario was constrained to the available well location that reflects their geological situation and tectonic framework. The Khatatba organofacies are classified as active/effective organic-rich interval since the Albian (~108.59 Ma, e.g. Lower Safa A-S7 at JD-4 well). Therefore, TOC values tend to be lower representing the residual TOC values more willingly than reflecting its initial TOC values, thus highlighting a high maturation level and expulsion. The oil window is related to basin burial at the JD-4 well rather than basin evolution at JG-2 well. Applying the petroleum generation kinetics for type II kerogen indicates that oil generation and wet gas windows (gas onset) initiated in the Early Cretaceous. The organofacies intervals (type II and type II/III kerogen) at JG-2 well have not attained a thermal-maturity level to generate secondary, associated thermogenic gas. The gas window (gas onset) initiated since (Early Cretaceous) ~105.35 Ma through the deposition of the Cretaceous Kharita sediments at JD-4 well.

The distribution of oil, gas, and mixed oil and (or) gas produced from the Khatatba Formation in the JG-2 well points to some significant trends that can be attributed to the thermal maturity of the Khatatba organofacies at the JD-4 well. The majority of the gas accumulations are found along the northwestern part (JG-2 well) at right angles to the NE-SW fault plan. The southeast part (JD-4 well) is deeper and more thermally mature. In addition, oil accumulations are concentrated at the JG-2 well, where thermal-maturity levels are low. Moreover, the lack of productive reservoirs in the southeastern part (JD-4 well) is attributable to the low-quality reservoirs as deduced from the petrophysical evaluation. This supposes that the accumulation of hydrocarbons (oil and/or gas) in the Khatatba Formation at JG-2 well possibly migrated and charged from the more mature/active organofacies at the JD-4 well since Early Cretaceous. Wherever, the initial expulsion of generated hydrocarbon from Khatatba-S7 has occurred.

Neither the Khatatba organofacies at the JG-2 well entered the gas windows nor do the hydrocarbon-bearing zones exhibit a cracking of oil in the reservoir owing to the low reservoir temperature. Therefore, the gas accumulation in the JG-2 well is not a product of the secondary cracking of entrapped liquid hydrocarbon that converted to gas in reservoirs. Consequently, the gas accumulations in Kabrit Member (JG-2 well) is interpreted to be co-generated from the generated oil (oil prone type II kerogen) at the JD-4 well. Then the co-generated gas subsequently migrated from JD-4 well northwestward into the porous Kabrit reservoirs perpendicular to the NE-SW faults.

The vertical/near vertical hydrocarbon migration pathways through NE-SW fault system from JD-4 well along with lateral migration were fundamental to the productivity of the JG-2 well. The tectonic framework of the NEAG concession is critical to hydrocarbon migration where the normal NE-SW

fault associated with fractures facilitate vertical migration. On the other hand, the stratigraphic surfaces and erosion enhanced lateral migration. The NE-SW faults control the depositional patterns, thermal maturation, migration pathway panels of the generated hydrocarbon and the distribution of oil-associated gas. The generated hydrocarbon (oil and/or gas) partially accumulated in the source rock and slightly adsorbed by the organic matter. A quantity of the expelled hydrocarbons accumulated in the reservoir however mostly misplaced through the migration pathways. Therefore, gas production from the oil-bearing zone of the Khatatba Formation possibly charged from northwestward-migrated oil from the JD-4 well.

Highlights

- The maximum burial, heating and mostly hydrocarbon generation occurred in the Cretaceous
- The oil window is associated with basin burial at JD-4 well rather than basin evolution at JG-2 well
- The Khatatba organofacies is classified as active/effective source rock at JD-4 well
- Oil and gas phases obtained at the JD-4 well while liquid phase is dominant at JG-2 well
- The phase of the generated hydrocarbon varies in relation to the level of thermal maturity and kerogen type
- Best accordance achieved with present-day heat flow values in the range of 26-40 mW/m^2

Acknowledgements

The authors are appreciative to the Egyptian General Petroleum Corporation (EGPC) and Badr El Din Petroleum Company (**BAPETCO**) for providing the materials, reports from their archives, and all the digital logs. The authors also acknowledge the Schlumberger Company for utilising PetroMod® software applications. The authors express thanks Dr **Haytham El-Atfy** for numerous discussions that improved the understanding of the basin development and geological situation. The authors are also very grateful for the comments and suggestions made by editor-in-chief and internal critical (potential) reviewers, which have significantly strengthened the article.

Disclosure statement

No potential conflict of interest was reported by the authors.

ORCID

Mohammed A. Ahmed http://orcid.org/0000-0001-5370-3779

References

Aal AE. 1988. Structural framework of Abu Gharadig basin Western Desert, Egypt. 9th Petroleum Exploration and Production Conference; Nov 20–23; Cairo: Egyptian General Petroleum Corporation.

Ahmed AM. 2008. Geodynamic evolution and petroleum system of Abu Gharadig Basin, north Western Desert, Egypt, Aachen, RWTH-Aachen University: [Dissertation].

Allen AP, Allen RJ. 1990. Basin analysis: principles and applications. Oxford: Blackwell Scientific Publications; p. 451.

Allen AP, Allen RJ. 2005. Basin analysis: principles and applications. Oxford: Blackwell Scientific Publications; p. 549.

Allen AP, Allen RJ. 2013. Basin analysis: principles and applications to petroleum play assessment. Malaysia: Blackwell Scientific Publications; p. 619.

Bayoumi T. 1996. The influence of interaction of depositional environment and synsedimentary tectonics on the development of some Late Cretaceous source rocks, Abu Gharadig basin, Western Desert, Egypt. 13th Petroleum Exploration and Production Conference. 2:475–496.

Bensley DF, Crelling JC. 1994. The inherent heterogeneity within the vitrinite maceral group. Fuel. 73:1306–1316.

Burrus, J., Osadetz, K., Wolf, S., et al., 1996. A two-dimensional regional basin model of Williston basin hydrocarbon systems. Am Assoc Pet Geol Bull. 80(2):265–291.

Durand, B., Alpern, B., Pittion, L. J., et al., 1986. Reflectance of vitrinite as a control of thermal history of sediments. 1st IFP Exploration Research Conferences; ; Carcans, France. p. 441–474

EGPC. 1992. Western Desert, oil and gas fields, a comprehensive overview. 11th Petroleum Exploration and Production Conference; Cairo: Egyptian General Petroleum Corporation. p. 1–431

El Diasty SW. 2015. Khatatba Formation as an active source rock for hydrocarbons in the northeast Abu Gharadig Basin, north Western Desert, Egypt. J Arabian Geosci. 8:1903–1920.

Guiraud R, Bosworth W. 1999. Phanerozoic geodynamic evolution of northeastern Africa and the northwestern Arabian platform. Tectonophysics. 315:73–108.

Guiraud R, Issawi B, Bosworth W. 1999. Phanerozoic history of Egypt and its surroundings. In: Ziegler PA, Cavazza W, Robertson AHF, editors. PeriTethyan rift/wrench basins and passive margins. Me´m. Mus. Natl. Hist. Nat., Publications Scientifiques, Diffusion, Paris, France. PeriTethys Memoir; p. 6.

Hantschel T, Kauerauf IA. 2009. Fundamentals of basin and petroleum systems modeling. Berlin: Springer-Verlag; p. 476.

Harland, B. W., Armstrong, R. R., Cox, V. A., et al. 1990. A Geologic time scale. Cambridge: Cambridge University Press; p. 1–131.

Hassan AMM, Taha AA, Issa IG. 2016. Petrophysical interpretation for reservoir characterization in north-east Abu Gharadig (NEAG), Western Desert-Egypt. Egypt J Appl Geophys. 15.

Heroux Y, Chagnon A, Bertrand R. 1979. Compilation and correlation of major thermal maturation indicators. Am Assoc Pet Geol Bull. 63:2128–2144.

Abd El Kireem, R. M., Schrank, E., Samir, et al. 1996. Cretaceous palaeoecology, palaeogeography and palaeoclimatology of the northern Western Desert, Egypt. J Afr Earth Sci. 22(1):93–112.

Kostandi AB. 1963. Eocene facies maps and tectonic interpretation in the Western Desert, Egypt. Revue De l'Institut Francais Du Petrole. 18(10):1331–1343.

Kubler, B., Pittion, J. L., Heroux, Y., et al. 1979. Sur le pouvoir reflecteur de la vitrinite dans quelques roches du Jura, de la Molasse et des Nappes prealpines, helvetiques et penniques (Suisse occidentale et Haute-Savoie). Eclogae Geologicae Helvetiae. 72(2):347–373.

Littke R, Leythaeuser D. 1993. Migration of oil and gas in coals. Am Assoc Pet Geol Stud Geol. 38:219–236.

Lüning, S., Kolonic, S., Belhadj, M. E., et al. 2004. Integrated depostional model for the Cenomanian –turonian organic – rich strat in North Africa. Earth Sci Rev. 64:51–117.

Magoon LB, Dow WG. 1994. The petroleum system-from source to trap. Am Assoc Pet Geol Memoir. 60:665.

Maky AF, Ramadan MAM. 2008. Nature of organic matter, thermal maturation and hydrocarbon potentiality of Khatatba Formation at East Abu Gharadig Basin, North Western Desert, Egypt. Aus J Basic Appl Sci. 2(2):194–209.

Meshref WM. 1990. Tectonic framework of Egypt. In: Said R, editor. Geology of Egypt. Rotterdam: Balkema; p. 113–156.

Meshref WM. 1996. Cretaceous tectonics and its impaction on oil exploration in regional Northern Egypt. Geol Soc Egypt. 2(Spec. Publ.):199–241.

Moustafa AR, El Badrawy R, Gibali H. 1998. Pervasive E–ENE oriented faults in northern Egypt and their effect on the development and inversion of prolific sedimentary basins. 14th Petroleum Conference. 1:51–67.

Moustafa RA. 2008. Mesozoic-Cenozoic basin evolution in the Northern Western Desert of Egypt. Geo East Libya. 3:29–46.

Palmer SE. 1993. Organic geochemistry of organic rich Cretaceous Carbonates with regard to depostional setting. Am Assoc Pet Geol Bull. 77(2):339.

Pepper SA, Corvi JP. 1995. Simple kinetic models of petroleum formation. Part I: oil and gas generation from kerogen. Mar Pet Geol. 12(3):291–319.

Price LC, Barker CE. 1985. Suppression of vitrinite reflectance in amorphous rich kerogen-a major unrecognized problem. J Pet Geol. 8(1):59–84.

RRI. 1982. Petroleum potential evaluation of the Western Desert, Egypt. (8 volumes): Unpublished report prepared for EGPC

Schlumberger. 1984. In Geology of Egypt (pp. 1–64). Paper presented at the Well Evaluation Conference, Schlumberger, Cairo.

Schlumberger. 1995. In Geology of Egypt (pp. 58–66). Paper presented at the Well Evaluation Conference, Schlumberger, Cairo.

Shalaby MR, Hakimi HH, Abdullah WH. 2011. Geochemical characteristics and hydrocarbon generation modeling of the Jurassic source rocks in the Shoushan Basin, north Western Desert, Egypt. Mar Pet Geol. 28:1611–1624.

Sweeney JJ, Burnham KA. 1990. Evaluation of a simple model of vitrinite reflectance based on chemical kinetics. Am Assoc Pet Geol Bull. 74(10):1559–1570.

Ungerer, P., Burrus, J., Doligez, B., et al. 1990. Basin evaluation by integrated two-dimensional modelling of heat transfer, fluid flow, hydrocarbon generation, and migration. Am Assoc Pet Geol Bull. 74(3):309–335.

Welte HD, Yükler M. 1981. Petroleum origin and accumulation in basin evolution- a quantitative model. Am Assoc Pet Geol Bull. 65:1387–1396.

Whelan KJ, Thomson Rizer LC. 1993. Chemical methods for assessing kerogen and protokerogen types and maturity. In: Engel MH, Macko AS, editors. Organic Geochemistry. New York: Plenum Press; p. 289–346.

Wygrala BP. 1989. Integrated study of an oil field in the southern Po basin, northern Italy, Köln, University of Köln: [Dissertation].

Zobaa, M. K., El Beialy, S. Y., El-Sheikh, H. A., et al. 2013. Jurassic-Cretaceous palynomorphs, palynofacies and petroleum potential of the Sharib-1x and Ghoroud-1x wells, north Western Desert, Egypt. J Afr Earth Sci. 78:51–65.